

Non-Singular Method of Fundamental Solutions for Two-Dimensional Isotropic Elasticity Problems

Q. G. Liu¹, and B. Šarler^{1 2 3 4}

Abstract: The purpose of the present paper is development of a Non-singular Method of Fundamental Solutions (NMFS) for two-dimensional isotropic linear elasticity problems. The NMFS is based on the classical Method of Fundamental Solutions (MFS) with regularization of the singularities. This is achieved by replacement of the concentrated point sources by distributed sources over circular discs around the singularity, as originally suggested by [Liu (2010)] for potential problems. The Kelvin's fundamental solution is employed in collocation of the governing plane strain force balance equations. In case of the displacement boundary conditions, the values of distributed sources are calculated directly and analytically. In case of traction boundary conditions, the respective desingularized values of the derivatives of the fundamental solution in the coordinate directions, as required in the calculations, are calculated indirectly from the considerations of two reference solutions of the linearly varying simple displacement fields. The developments represent a first use of NMFS for solid mechanics problems. With this, the main drawback of MFS for these types of problems is removed, since the artificial boundary is not present. In order to demonstrate the feasibility and accuracy of the newly developed method, is the NMFS solution compared to the MFS solution and analytical solutions for a spectra of plane strain elasticity problems, including bi-material problems. NMFS turns out to give similar results than the MFS in all spectra of performed tests. The lack of artificial boundary is particularly advantageous for using NMFS in multi-body problems.

Keywords: isotropic elasticity; plane strain; Navier's equation; displacement and traction boundary conditions; Kelvin's fundamental solution; MFS; Non-singular MFS.

¹ University of Nova Gorica , Nova Gorica, Slovenia.

² Institute of Metals and Technology, Ljubljana, Slovenia.

³ COBIK, Solkan, Slovenia.

⁴ Corresponding author: Professor Božidar Šarler (bozidar.sarler@ung.si, bozidar.sarler@imt.si, bozidar.sarler@cobik.si)

1 Introduction

The main idea of MFS [Chen; Karageorghis and Smyrlis (2008)] consists of approximating the solution of the partial differential equation by a linear combination of fundamental solutions, defined in source points. The expansion coefficients are calculated by collocation or least squares fit of the boundary conditions. The fundamental solution is for certain PDE's singular in the source points and this is the reason why the source points have to be located outside the domain in the classical MFS for such situations. Then, the original problem is reduced to determining the unknown coefficients of the fundamental solutions and the coordinates of the source points by requiring the approximation to satisfy the boundary conditions and hence solving a non-linear problem. If the source points are a priori fixed (on a fictitious boundary) then the coefficients of the approximation are determined by solving a linear problem.

The MFS has become very popular in recent years because of its simplicity. Clearly, it is applicable when the fundamental solution of the partial differential operator of the governing equation (or of the system of governing equations) of the problem under consideration is known. Probably, the most important advantage of the method over other boundary methods, such as the boundary element method (BEM), is the ease with which it can be implemented, since it does not involve numerical integration. The MFS has been successfully applied to a large variety of physical problems. A review of such applications as well as the assessment of advantages of the method over other methods can be found in [Fairweather and Karageorghis (1998); Golberg and Chen (1997; 1999); Kolodziej (1987; 2001)]. The method has been widely used for the solution of problems in linear elasticity. The first application of the MFS for elasticity problems can be found in the paper [Kupradze and Aleksidze (1964)], whereas a theoretical analysis and density results for problems of linear elasticity may be found in the papers [Kupradze (1964); Smyrlis (2009)]. The solution of anisotropic elasticity problems was considered in the paper [Berger and Karageorghis (2001); Maharejin (1985)]. In the paper [Marin and Lesnic (2004)], inverse problems in planar elasticity were considered whereas axisymmetric elastic problems were studied in the papers [Redekop and Thompson (1983); Karageorghis and Fairweather (2000)]. The MFS has been applied to the computation of stress intensity factors in linear elastic fracture mechanics [Berger, Karageorghis and Martin (2007); Karageorghis, Poullikkas and Berger (2006)] as well. The MFS was applied to thermo-elasticity problems in [Aleksidze (1991); Kupradze, Gegelia, Bashaeshvili and Burchuladze (1976)]. Further applications of the MFS to elasticity problems can be found in [Patterson and Sheikh (1982); Redekop (1982); Burgess and Maharejin (1984); Redekop and Cheung (1987); Raamachandran and Rajamohan (1996); Fenner (2001); Poullikkas and Karageorghis

(2002); Tsai (2007); Marin (2011)]. Multi-domain (multi-zone) formulations play an important part in numerical analysis when dealing with problems involving interfaces or dissimilar materials, such as composite materials, etc. Berger and Karageorghis (2001) present the MFS for multi-domain anisotropic elasticity problems. In the traditional MFS, the fictitious boundary, positioned outside the problem domain, is required to place the source points. This avoids the singularity of the solution at the boundary which would prevent the proper compliance with the boundary conditions. The determination of the distance between the real boundary and the fictitious boundary is based on experience and therefore troublesome. In recent years, various efforts have been made, aiming to remove this drawback of the MFS, so that the source points can be placed on the real boundary directly. Young, Chen and Lee (2005); Young, Chen, Chen and Kao (2007); Chen, Kao, Chen, Young and Lu (2006) proposed to place the source points on the boundary in the MFS. They introduce novel ways to determine the diagonal collocation matrix coefficients. The diagonal coefficients were determined directly for simple geometries or by using the results from the BEM, based on the fact that the MFS and the indirect boundary integral formulation are similar in nature. In their approach, information of the neighboring points before and after each source point is needed, in order to form line segments for integrating the kernels to obtain the diagonal coefficients. This is essentially the same information of the element connectivity as in a BEM mesh. Šarler (2009) proposed a similar modified MFS, where the diagonal terms are determined by the integration of the fundamental solution on the line segments formed by using neighboring points, and the use of a constant solution to determine the diagonal coefficients of the derivatives of the fundamental solution in different coordinate directions. This approach is very stable, but it amounts to solve the problem twice. Chen and Wang (2010) proposed a similar method for determining the diagonal coefficients in the modified MFS by applying a known solution inside the domain, so that the diagonal coefficients from both the fundamental solution and its derivative can be determined indirectly, without using any element or integration concept. Again, this approach is appealing, stable, and accurate but it is costly for solving large-scale problems due to the need to solve the problem twice. The solution also depends on the choice of the reference points. Gu, Chen and Zhang (2011) applied the singular boundary method to two-dimensional (2D) elasticity problems, in which they use an inverse interpolation technique to regularize the singularity of the fundamental solution of the equation governing the problem of interest. Chen, Lin and Wang (2011) developed the regularized meshless method also for the nonhomogeneous problems in conjunction with the dual reciprocity technique in the evaluation of the particular solution. Liu (2010) recently presented a new boundary meshfree approach based on the modified MFS that has

no fictitious boundaries and singularities. In the new approach, the concentrated point sources are replaced with area-distributed sources covering the source points for 2D problems. These area-distributed sources represent analytical integration of the original singular fundamental solution, so that they preserve the advantage of diagonal dominance for the system of equations, while they have no troublesome singularity issues. Liu (2010) called the method boundary distributed source (BDS) method. Liu (2010) used the approach of Šarler (2009) to determine the diagonal coefficients of the derivatives of the fundamental solution. Liu's approach has been recently extended to solve porous media problems with moving boundaries [Perne, Šarler and Gabrovšek (2012)]. In the present paper, we use a Non-singular MFS, based on Liu (2010), to deal with the 2D isotropic elasticity problems. We respectively use area-distributed sources covering the source points to replace the concentrated point sources. This NMFS approach also does not require a detailed information about the neighboring points for each source point, thus it is a truly meshfree boundary method. The derivatives of the fundamental solution in the distributed source points are calculated by adopting the methodology by Šarler (2009) from the Laplace to Kelvin fundamental solution. The rest of the paper is structured as follows. Solution procedure is elaborated for MFS and NMFS in a uniform way. Numerical examples of different type of deformations with analytical solutions are presented to demonstrate the feasibility and accuracy of the NMFS, followed by bi-material examples. At the end, the conclusions and further research directions are given.

2 Governing Equations

Consider a two-dimensional solid in domain Ω with boundary Γ . The solid behaves ideally isotropic elastic. Let us introduce a two-dimensional Cartesian coordinate system with orthonormal base vectors \mathbf{i}_x and \mathbf{i}_y , and coordinates p_x and p_y of point P with position vector $\mathbf{p} = p_x\mathbf{i}_x + p_y\mathbf{i}_y$. The solid is governed by Navier's equations for plane strain problems, which are the conditions for equilibrium, expressed with the displacement \mathbf{u}

$$\frac{2(1-\nu)}{1-2\nu} \frac{\partial^2 u_x(\mathbf{p})}{\partial p_x^2} + \frac{\partial^2 u_x(\mathbf{p})}{\partial p_y^2} + \frac{1}{1-2\nu} \frac{\partial^2 u_y(\mathbf{p})}{\partial p_x \partial p_y} = 0, \quad (1)$$

$$\frac{2(1-\nu)}{1-2\nu} \frac{\partial^2 u_y(\mathbf{p})}{\partial p_y^2} + \frac{\partial^2 u_y(\mathbf{p})}{\partial p_x^2} + \frac{1}{1-2\nu} \frac{\partial^2 u_x(\mathbf{p})}{\partial p_x \partial p_y} = 0, \quad \mathbf{p} \in \Omega \cup \Gamma, \quad (2)$$

where ν is Poisson's ratio. The boundary is divided into two not necessarily connected parts $\Gamma = \Gamma^D + \Gamma^T$. On the part Γ^D the displacement (Dirichlet) boundary conditions are given, and on the part Γ^T the traction (Neumann) boundary conditions are given. (see Fig. 1)

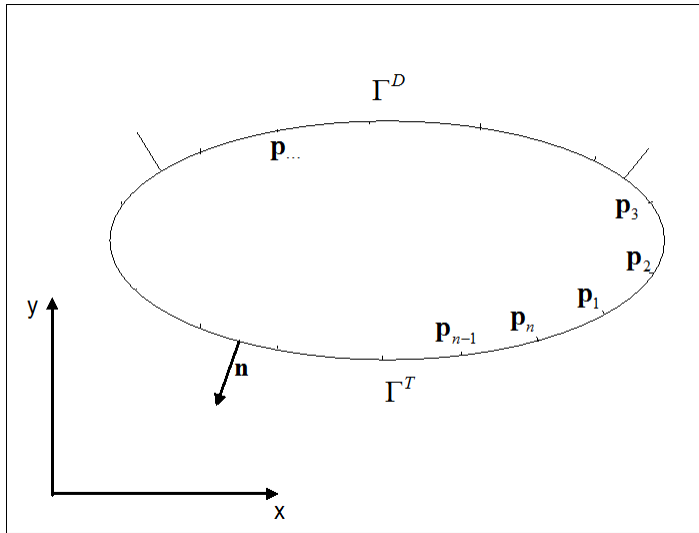


Figure 1: Problem domain Ω with displacement (Dirichlet) Γ^D and traction (Neumann) Γ^T parts of the boundary.

$$u_\zeta(\mathbf{p}) = \bar{u}_\zeta(\mathbf{p}); \quad \zeta = x, y, \quad \mathbf{p} \in \Gamma^D, \quad (3)$$

$$t_\zeta(\mathbf{p}) = \bar{t}_\zeta(\mathbf{p}); \quad \zeta = x, y, \quad \mathbf{p} \in \Gamma^T, \quad (4)$$

where \bar{u}_ζ and \bar{t}_ζ represent known functions. The strains $\varepsilon_{\zeta\xi}$; $\zeta, \xi = x, y$ are related to the displacement gradients by

$$\varepsilon_{\zeta\xi} = \frac{1}{2} \left(\frac{\partial u_\zeta}{\partial p_\xi} + \frac{\partial u_\xi}{\partial p_\zeta} \right). \quad (5)$$

The stress components $\sigma_{\zeta\xi}$; $\zeta, \xi = x, y$ are for the plane strain cases related to the strains through Hooke's law

$$\sigma_{\zeta\xi} = \lambda \delta_{\zeta\xi} (\varepsilon_{xx} + \varepsilon_{yy}) + 2\mu \varepsilon_{\zeta\xi}, \quad (6)$$

where $\mu = E/2(1 + \nu)$ is the shear modulus of elasticity, E is modulus of elasticity, or Young's modulus, $\lambda = 2\nu\mu/(1 - 2\nu)$ is Lamé constant, and $\delta_{\zeta\xi}$ is the Kronecker delta

$$\delta_{\zeta\xi} = \begin{cases} 1, & \zeta = \xi \\ 0, & \zeta \neq \xi \end{cases}. \quad (7)$$

The formulation for plan stress can be obtained by introducing the modified Poisson's coefficient ν' and modified Young's modulus E' , defined as

$$\nu' = \frac{\nu}{1 + \nu}, \quad E' = E \left[1 - \left(\frac{\nu}{1 + \nu} \right)^2 \right]. \quad (8)$$

The tractions t_x and t_y are defined in terms of the stresses as

$$t_\zeta = \sigma_{\zeta x} n_x + \sigma_{\zeta y} n_y, \quad \zeta = x, y, \quad (9)$$

where n_x and n_y denote the coordinates of the outward normal \mathbf{n} at the boundary point \mathbf{p} .

3 Solution procedure

3.1 Fundamental solution

Kelvin's fundamental solution of elasticity is given (see [Beskos (1987)]) in two dimensional plane strain situation by

$$U_{\zeta\xi}(\mathbf{p}, \mathbf{s}) = \frac{1}{8\pi\mu(1-\nu)} \left\{ (3-4\nu) \log\left(\frac{1}{r}\right) \delta_{\zeta\xi} + \frac{(p_\zeta - s_\zeta)(p_\xi - s_\xi)}{r^2} \right\}, \quad (10)$$

$\zeta, \xi = x, y,$

where $U_{\zeta\xi}(\mathbf{p}, \mathbf{s})$ represents the displacement in the direction ζ at point \mathbf{p} due to a unit point force acting in the direction ξ at point \mathbf{s} . $r = \sqrt{(p_x - s_x)^2 + (p_y - s_y)^2}$ is the distance between the point \mathbf{p} and the source point \mathbf{s} . The solution (10) is expanded as follows

$$U_{xx}(\mathbf{p}, \mathbf{s}) = \frac{1}{8\pi\mu(1-\nu)} \left\{ (3-4\nu) \log\left(\frac{1}{r}\right) + \frac{(p_x - s_x)^2}{r^2} \right\}, \quad (11)$$

$$U_{xy}(\mathbf{p}, \mathbf{s}) = U_{yx}(\mathbf{p}, \mathbf{s}) = \frac{1}{8\pi\mu(1-\nu)} \frac{(p_x - s_x)(p_y - s_y)}{r^2}, \quad (12)$$

$$U_{yy}(\mathbf{p}, \mathbf{s}) = \frac{1}{8\pi\mu(1-\nu)} \left\{ (3-4\nu) \log\left(\frac{1}{r}\right) + \frac{(p_y - s_y)^2}{r^2} \right\}. \quad (13)$$

It can be shown that the following u_x and u_y satisfy the governing Eqs. (1,2)

$$u_x(\mathbf{p}) = U_{xx}(\mathbf{p}, \mathbf{s})\alpha + U_{xy}(\mathbf{p}, \mathbf{s})\beta, \quad (14)$$

$$u_y(\mathbf{p}) = U_{yx}(\mathbf{p}, \mathbf{s})\alpha + U_{yy}(\mathbf{p}, \mathbf{s})\beta, \quad (15)$$

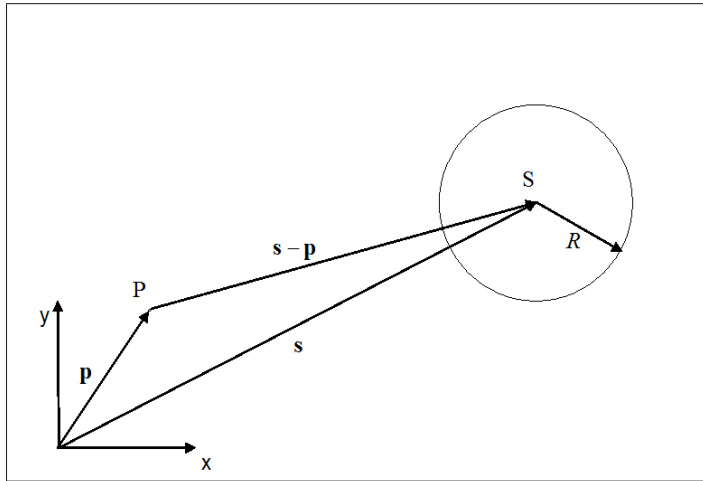


Figure 2: Distributed source on a circle $A(\mathbf{s}, R)$ with radius R .

where α and β represent arbitrary constants. The fundamental solution $U_{\zeta\xi}(\mathbf{p}, \mathbf{s})$ is singular when $\mathbf{p} = \mathbf{s}$. We use the desingularization technique, proposed by Liu (2010), for evaluating the singular values. We modify his approach in the sense of preserving the original fundamental solution in all points except near the singularity, and by scaling the singularity with the area of the circle over which the desingularization integration is performed. This allows us to treat the MFS and the NMFS in a formally same way. The desingularization (transformation of $U_{\zeta\xi}(\mathbf{p}, \mathbf{s})$ into $\tilde{U}_{\zeta\xi}(\mathbf{p}, \mathbf{s})$) is performed in two steps:

$$U'_{\zeta\xi}(\mathbf{p}, \mathbf{s}) = \begin{cases} U_{\zeta\xi}(\mathbf{p}, \mathbf{s}); & r > R \\ \frac{1}{\pi R^2} \int_{A(\mathbf{s}, R)} U_{\zeta\xi}(\mathbf{p}, \mathbf{s}) dA; & r \leq R \end{cases}, \quad (16)$$

where $A(\mathbf{s}, R)$ represents a circle with radius R , centered around \mathbf{s} . The involved integrals can be calculated as follows (by using the integration in polar coordinates $p_x - s_x = r \cos \theta$, $p_y - s_y = r \sin \theta$)

$$\frac{1}{\pi R^2} \int_{A(\mathbf{s}, R)} U_{\zeta\xi}(\mathbf{p}, \mathbf{s}) dA = \frac{1}{\pi R^2} \int_0^{2\pi} \int_0^R U_{\zeta\xi}(\mathbf{p}, \mathbf{s}) r dr d\theta, \quad (17)$$

$$\begin{aligned} \frac{1}{\pi R^2} \int_{A(s,R)} U_{xx}(\mathbf{p}, \mathbf{s}) dA &= \frac{1}{\pi R^2} \int_{A(s,R)} U_{yy}(\mathbf{p}, \mathbf{s}) dA \\ &= \frac{1}{8\pi\mu(1-\nu)} \left((3-4\nu) \log\left(\frac{1}{R}\right) + 2(1-\nu) \right), \end{aligned} \tag{18}$$

$$\frac{1}{\pi R^2} \int_{A(s,R)} U_{xy}(\mathbf{p}, \mathbf{s}) dA = \frac{1}{\pi R^2} \int_{A(s,R)} U_{yx}(\mathbf{p}, \mathbf{s}) dA = 0. \tag{19}$$

In order to impose smoothness of the desingularized value of the fundamental solution and its derivatives at point $r = R$, Liu (2010) used an additional term $-r^2/4$ inside the circular disc, with a remark in the discussion, that the desingularized fundamental solution inside the disc does not satisfy the governing equation. This is acceptable, since the dimension of R is usually much smaller than a typical distance between the boundary nodes. However, the values inside the disc, except at $r = 0$ have never been used in his calculations. In a similar way, in order to match $U_{\zeta\xi}(\mathbf{p}, \mathbf{s}) = U'_{\zeta\xi}(\mathbf{p}, \mathbf{s})$ and $\frac{\partial}{\partial p_\zeta} U_{\zeta\xi}(\mathbf{p}, \mathbf{s}) = \frac{\partial}{\partial p_\zeta} U'_{\zeta\xi}(\mathbf{p}, \mathbf{s})$, when $r = R$, we modify

$$\tilde{U}_{\zeta\xi}(\mathbf{p}, \mathbf{s}) = \begin{cases} U_{\zeta\xi}(\mathbf{p}, \mathbf{s}); & r > R \\ U_{\zeta\xi}(\mathbf{p}, \mathbf{s}); & r \leq R \end{cases}, \tag{20}$$

where

$$\begin{aligned} \tilde{U}_{xx}(\mathbf{p}, \mathbf{s}) &= \frac{1}{8\pi\mu(1-\nu)} \left((3-4\nu) \log\left(\frac{1}{R}\right) + 2(1-\nu) \frac{R^2-r^2}{R^2} + \frac{(p_x-s_x)^2 r^2}{R^4} \right. \\ &\quad \left. + \frac{[3(p_x-s_x)^2 - (p_y-s_y)^2][(R^2-r^2)r^2]}{2R^6} \right), \end{aligned} \tag{21}$$

$$\begin{aligned} \tilde{U}_{yy}(\mathbf{p}, \mathbf{s}) &= \frac{1}{8\pi\mu(1-\nu)} \left((3-4\nu) \log\left(\frac{1}{R}\right) + 2(1-\nu) \frac{R^2-r^2}{R^2} + \frac{(p_y-s_y)^2 r^2}{R^4} \right. \\ &\quad \left. + \frac{[3(p_y-s_y)^2 - (p_x-s_x)^2][(R^2-r^2)r^2]}{2R^6} \right) \end{aligned} \tag{22}$$

$$\begin{aligned} \tilde{U}_{xy}(\mathbf{p}, \mathbf{s}) = \tilde{U}_{yx}(\mathbf{p}, \mathbf{s}) &= \frac{1}{8\pi\mu(1-\nu)} \left[\frac{(p_x-s_x)(p_y-s_y)r^2}{R^4} \right. \\ &\quad \left. + \frac{[2(p_x-s_x)(p_y-s_y)][(R^2-r^2)r^2]}{R^6} \right]. \end{aligned} \tag{23}$$

This forms than give smoothness of the desingularized and singular fundamental solution and their derivatives at $r = R$ and at the same time preserve the desingularized value at $r = 0$. It can also be shown that the following u_x and u_y satisfy the governing Eqs. (1, 2)

$$u_x(\mathbf{p}) = \tilde{U}_{xx}(\mathbf{p}, \mathbf{s})\alpha + \tilde{U}_{xy}(\mathbf{p}, \mathbf{s})\beta, \tag{24}$$

$$u_y(\mathbf{p}) = \tilde{U}_{yx}(\mathbf{p}, \mathbf{s})\alpha + \tilde{U}_{yy}(\mathbf{p}, \mathbf{s})\beta, \quad \mathbf{p} \notin A(s, R) \tag{25}$$

3.2 Discretisation

The solution of the problem is sought in the form

$$u_x(\mathbf{p}) = \sum_{n=1}^N U_{xx}(\mathbf{p}, \mathbf{p}_n)\alpha_n + \sum_{n=1}^N U_{xy}(\mathbf{p}, \mathbf{p}_n)\beta_n, \tag{26}$$

$$u_y(\mathbf{p}) = \sum_{n=1}^N U_{yx}(\mathbf{p}, \mathbf{p}_n)\alpha_n + \sum_{n=1}^N U_{yy}(\mathbf{p}, \mathbf{p}_n)\beta_n \quad \mathbf{p} \notin \bigcup_{n=1}^N A(\mathbf{p}_n, R). \tag{27}$$

Because of Eqs. (5, 6, 9), the traction can be expressed as

$$t_x(\mathbf{p}) = \sum_{n=1}^N T_{xx}(\mathbf{p}, \mathbf{p}_n)\alpha_n + \sum_{n=1}^N T_{xy}(\mathbf{p}, \mathbf{p}_n)\beta_n, \tag{28}$$

$$t_y(\mathbf{p}) = \sum_{n=1}^N T_{yx}(\mathbf{p}, \mathbf{p}_n)\alpha_n + \sum_{n=1}^N T_{yy}(\mathbf{p}, \mathbf{p}_n)\beta_n, \quad \mathbf{p} \notin \bigcup_{n=1}^N A(\mathbf{p}_n, R) \tag{29}$$

where

$$T_{xx}(\mathbf{p}, \mathbf{p}_n) = \left[\frac{2\mu(1-\nu)}{1-2\nu} \frac{\partial U_{xx}(\mathbf{p}, \mathbf{p}_n)}{\partial p_x} + \frac{2\mu\nu}{1-2\nu} \frac{\partial U_{yx}(\mathbf{p}, \mathbf{p}_n)}{\partial p_y} \right] n_{nx} + \left[\mu \frac{\partial U_{xx}(\mathbf{p}, \mathbf{p}_n)}{\partial p_y} + \mu \frac{\partial U_{yx}(\mathbf{p}, \mathbf{p}_n)}{\partial p_x} \right] n_{ny}, \tag{30}$$

$$T_{xy}(\mathbf{p}, \mathbf{p}_n) = \left[\frac{2\mu(1-\nu)}{1-2\nu} \frac{\partial U_{xy}(\mathbf{p}, \mathbf{p}_n)}{\partial p_x} + \frac{2\mu\nu}{1-2\nu} \frac{\partial U_{yy}(\mathbf{p}, \mathbf{p}_n)}{\partial p_y} \right] n_{nx} + \left[\mu \frac{\partial U_{xy}(\mathbf{p}, \mathbf{p}_n)}{\partial p_y} + \mu \frac{\partial U_{yy}(\mathbf{p}, \mathbf{p}_n)}{\partial p_x} \right] n_{ny}, \tag{31}$$

$$T_{yx}(\mathbf{p}, \mathbf{p}_n) = \left[\mu \frac{\partial U_{yx}(\mathbf{p}, \mathbf{p}_n)}{\partial p_x} + \mu \frac{\partial U_{xx}(\mathbf{p}, \mathbf{p}_n)}{\partial p_y} \right] n_{nx} + \left[\frac{2\mu(1-\nu)}{1-2\nu} \frac{\partial U_{yx}(\mathbf{p}, \mathbf{p}_n)}{\partial p_y} + \frac{2\mu\nu}{1-2\nu} \frac{\partial U_{xx}(\mathbf{p}, \mathbf{p}_n)}{\partial p_x} \right] n_{ny}, \tag{32}$$

$$T_{yy}(\mathbf{p}, \mathbf{p}_n) = \left[\mu \frac{\partial U_{yy}(\mathbf{p}, \mathbf{p}_n)}{\partial p_x} + \mu \frac{\partial U_{xy}(\mathbf{p}, \mathbf{p}_n)}{\partial p_y} \right] n_{nx} + \left[\frac{2\mu(1-\nu)}{1-2\nu} \frac{\partial U_{yy}(\mathbf{p}, \mathbf{p}_n)}{\partial p_y} + \frac{2\mu\nu}{1-2\nu} \frac{\partial U_{xy}(\mathbf{p}, \mathbf{p}_n)}{\partial p_x} \right] n_{ny}, \tag{33}$$

where p_n represent N points, placed on artificial boundary, in case of MFS. The forms (30-33) with $U_{\zeta\xi}(\mathbf{p}, \mathbf{p}_n)$ and $T_{\zeta\xi}(\mathbf{p}, \mathbf{p}_n)$ replaced by $\tilde{U}_{\zeta\xi}(\mathbf{p}, \mathbf{p}_n)$ and $\tilde{T}_{\zeta\xi}(\mathbf{p}, \mathbf{p}_n)$ stand for NMFS formulation, where in this case \mathbf{p}_n represent N points, placed on the physical boundary. The explicit expressions, used in calculation of the traction boundary conditions, are

$$\frac{\partial U_{xx}(\mathbf{p}, \mathbf{s})}{\partial p_x} = \frac{1}{8\pi\mu(1-\nu)} \left[(4\nu-3) \frac{p_x-s_x}{r^2} + \frac{2(p_x-s_x)(p_y-s_y)^2}{r^4} \right], \tag{34}$$

$$\frac{\partial U_{xx}(\mathbf{p}, \mathbf{s})}{\partial p_y} = \frac{1}{8\pi\mu(1-\nu)} \left[(4\nu-3) \frac{p_y-s_y}{r^2} - \frac{2(p_y-s_y)(p_x-s_x)^2}{r^4} \right], \tag{35}$$

$$\frac{\partial U_{xy}(\mathbf{p}, \mathbf{s})}{\partial p_x} = \frac{\partial U_{yx}(\mathbf{p}, \mathbf{s})}{\partial p_x} = \frac{1}{8\pi\mu(1-\nu)} \frac{(p_y-s_y)[(p_y-s_y)^2 - (p_x-s_x)^2]}{r^4}, \tag{36}$$

$$\frac{\partial U_{yy}(\mathbf{p}, \mathbf{s})}{\partial p_x} = \frac{1}{8\pi\mu(1-\nu)} \left[(4\nu-3) \frac{(p_x-s_x)}{r^2} - \frac{2(p_x-s_x)(p_y-s_y)^2}{r^4} \right], \tag{37}$$

$$\frac{\partial U_{yy}(\mathbf{p}, \mathbf{s})}{\partial p_y} = \frac{1}{8\pi\mu(1-\nu)} \left[(4\nu-3) \frac{(p_y-s_y)}{r^2} + \frac{2(p_y-s_y)(p_x-s_x)^2}{r^4} \right], \tag{38}$$

$$\frac{\partial U_{xy}(\mathbf{p}, \mathbf{s})}{\partial p_y} = \frac{\partial U_{yx}(\mathbf{p}, \mathbf{s})}{\partial p_y} = \frac{1}{8\pi\mu(1-\nu)} \frac{(p_x-s_x)[(p_x-s_x)^2 - (p_y-s_y)^2]}{r^4}. \tag{39}$$

except at $\mathbf{p} = \mathbf{s}$, where the derivatives are calculated in an indirect way. The coefficients α_n and β_n are calculated from a system of $2N$ algebraic equations

$$\mathbf{Ax} = \mathbf{b}, \tag{40}$$

where \mathbf{A} stands for a $2N \times 2N$ matrix with the entries A_{ij} , \mathbf{x} is a $2N \times 1$ vector with the entries x_i , and \mathbf{b} is a $2N \times 1$ vector with entries b_i ,

$$A_{ij} = \chi_x^D(\mathbf{p}_i) \tilde{U}_{xx}(\mathbf{p}_i, \mathbf{p}_j) + \chi_x^T(\mathbf{p}_i) \tilde{T}_{xx}(\mathbf{p}_i, \mathbf{p}_j),$$

$$A_{i(N+j)} = \chi_x^D(\mathbf{p}_i) \tilde{U}_{xy}(\mathbf{p}_i, \mathbf{p}_j) + \chi_x^T(\mathbf{p}_i) \tilde{T}_{xy}(\mathbf{p}_i, \mathbf{p}_j), \tag{41}$$

$$A_{(N+i)j} = \chi_y^D(\mathbf{p}_i) \tilde{U}_{yx}(\mathbf{p}_i, \mathbf{p}_j) + \chi_y^T(\mathbf{p}_i) \tilde{T}_{yx}(\mathbf{p}_i, \mathbf{p}_j),$$

$$A_{(N+i)(N+j)} = \chi_y^D(\mathbf{p}_i) \tilde{U}_{yy}(\mathbf{p}_i, \mathbf{p}_j) + \chi_y^T(\mathbf{p}_i) \tilde{T}_{yy}(\mathbf{p}_i, \mathbf{p}_j), i, j = 1, 2, \dots, N. \tag{42}$$

$$\begin{aligned}
 b_i &= \chi^D(\mathbf{p}_i)u_x(\mathbf{p}_i) + \chi^T(\mathbf{p}_i)t_x(\mathbf{p}_i), b_{(N+i)} \\
 &= \chi^D(\mathbf{p}_i)u_y(\mathbf{p}_i) + \chi^T(\mathbf{p}_i)t_y(\mathbf{p}_i), i = 1, 2, \dots, N.
 \end{aligned}
 \tag{43}$$

where the displacement $\chi_\zeta^D, \zeta = x, y$ and the traction $\chi_\zeta^T, \zeta = x, y$ type of boundary conditions indicators are

$$\begin{aligned}
 \chi_\zeta^D(\mathbf{p}) &= \begin{cases} 1; & \mathbf{p} \in \Gamma^D \text{ in } \mathbf{i}_\zeta \text{ direction} \\ 0; & \mathbf{p} \notin \Gamma^D \text{ in } \mathbf{i}_\zeta \text{ direction} \end{cases}, \\
 \chi_\zeta^T(\mathbf{p}) &= \begin{cases} 1; & \mathbf{p} \in \Gamma^T \text{ in } \mathbf{i}_\zeta \text{ direction} \\ 0; & \mathbf{p} \notin \Gamma^T \text{ in } \mathbf{i}_\zeta \text{ direction} \end{cases}.
 \end{aligned}
 \tag{44}$$

The diagonal terms $\tilde{T}_{\zeta\xi}(\mathbf{p}_m, \mathbf{p}_m), \zeta, \xi = x, y, m = 1, \dots, N$ in Eqs. (28, 29) are in case of NMFS determined indirectly for collocation points on Γ^T . For this purpose, the method proposed by Šarler (2009) for potential problems, is applied to determine the diagonal terms in these equations. We assume two simple solutions in this approach, modified to cope with elasticity problems. The first simple solution is $\bar{u}_x(\mathbf{p}) = p_x + c_x, \bar{u}_y(\mathbf{p}) = 0$, everywhere, and c_x denotes a constant. It follows from the first solution

$$\frac{\partial u_x(\mathbf{p})}{\partial p_x} = 1, \frac{\partial u_x(\mathbf{p})}{\partial p_y} = \frac{\partial u_y(\mathbf{p})}{\partial p_x} = \frac{\partial u_y(\mathbf{p})}{\partial p_y} = 0.
 \tag{45}$$

It follows from Eq. (26) for the first solution

$$\frac{\partial \bar{u}_x(\mathbf{p})}{\partial p_x} = \sum_{n=1}^N \frac{\partial \tilde{U}_{xx}(\mathbf{p}, \mathbf{p}_n)}{\partial p_x} \alpha_n^1 + \sum_{n=1}^N \frac{\partial \tilde{U}_{xy}(\mathbf{p}, \mathbf{p}_n)}{\partial p_x} \beta_n^1 = 1,
 \tag{46}$$

$$\frac{\partial \bar{u}_x(\mathbf{p})}{\partial p_y} = \sum_{n=1}^N \frac{\partial \tilde{U}_{xx}(\mathbf{p}, \mathbf{p}_n)}{\partial p_y} \alpha_n^1 + \sum_{n=1}^N \frac{\partial \tilde{U}_{xy}(\mathbf{p}, \mathbf{p}_n)}{\partial p_y} \beta_n^1 = 0.
 \tag{47}$$

It follows from Eq. (27) for the first solution

$$\frac{\partial \bar{u}_y(\mathbf{p})}{\partial p_x} = \sum_{n=1}^N \frac{\partial \tilde{U}_{yx}(\mathbf{p}, \mathbf{p}_n)}{\partial p_x} \alpha_n^1 + \sum_{n=1}^N \frac{\partial \tilde{U}_{yy}(\mathbf{p}, \mathbf{p}_n)}{\partial p_x} \beta_n^1 = 0,
 \tag{48}$$

$$\frac{\partial \bar{u}_y(\mathbf{p})}{\partial p_y} = \sum_{n=1}^N \frac{\partial \tilde{U}_{yx}(\mathbf{p}, \mathbf{p}_n)}{\partial p_y} \alpha_n^1 + \sum_{n=1}^N \frac{\partial \tilde{U}_{yy}(\mathbf{p}, \mathbf{p}_n)}{\partial p_y} \beta_n^1 = 0.
 \tag{49}$$

We solve these equations for the corresponding α_n^1 and β_n^1 . The second simple solution is $\bar{u}_x(\mathbf{p}) = 0, \bar{u}_y(\mathbf{p}) = p_y + c_y$, everywhere, and c_y denotes a constant. It follows from the second solution

$$\frac{\partial u_x(\mathbf{p})}{\partial p_x} = \frac{\partial u_x(\mathbf{p})}{\partial p_y} = \frac{\partial u_y(\mathbf{p})}{\partial p_x} = 0, \frac{\partial u_y(\mathbf{p})}{\partial p_y} = 1.
 \tag{50}$$

It follows from Eq. (26) for the second solution

$$\frac{\partial \bar{u}_x(\mathbf{p})}{\partial p_x} = \sum_{n=1}^N \frac{\partial \tilde{U}_{xx}(\mathbf{p}, \mathbf{p}_n)}{\partial p_x} \alpha_n^2 + \sum_{n=1}^N \frac{\partial \tilde{U}_{xy}(\mathbf{p}, \mathbf{p}_n)}{\partial p_x} \beta_n^2 = 0, \quad (51)$$

$$\frac{\partial \bar{u}_x(\mathbf{p})}{\partial p_y} = \sum_{n=1}^N \frac{\partial \tilde{U}_{xx}(\mathbf{p}, \mathbf{p}_n)}{\partial p_y} \alpha_n^2 + \sum_{n=1}^N \frac{\partial \tilde{U}_{xy}(\mathbf{p}, \mathbf{p}_n)}{\partial p_y} \beta_n^2 = 0. \quad (52)$$

It follows from Eq. (27) for the second solution

$$\frac{\partial \bar{u}_y(\mathbf{p})}{\partial p_x} = \sum_{n=1}^N \frac{\partial \tilde{U}_{yx}(\mathbf{p}, \mathbf{p}_n)}{\partial p_x} \alpha_n^2 + \sum_{n=1}^N \frac{\partial \tilde{U}_{yy}(\mathbf{p}, \mathbf{p}_n)}{\partial p_x} \beta_n^2 = 0, \quad (53)$$

$$\frac{\partial \bar{u}_y(\mathbf{p})}{\partial p_y} = \sum_{n=1}^N \frac{\partial \tilde{U}_{yx}(\mathbf{p}, \mathbf{p}_n)}{\partial p_y} \alpha_n^2 + \sum_{n=1}^N \frac{\partial \tilde{U}_{yy}(\mathbf{p}, \mathbf{p}_n)}{\partial p_y} \beta_n^2 = 1. \quad (54)$$

We solve them for the corresponding α_n^2 and β_n^2 . The unknown 8 values of the derivatives of the fundamental solutions can respectively be calculated as follows. The equations (46,51) are used to obtain:

$$\frac{\partial \tilde{U}_{xx}(\mathbf{p}_m, \mathbf{p}_m)}{\partial p_x} = \frac{1}{\alpha_m^1 \beta_m^2 - \alpha_m^2 \beta_m^1} \left[\beta_m^2 - \sum_{n=1, n \neq m}^N \left((\alpha_n^1 \beta_m^2 - \alpha_n^2 \beta_m^1) \frac{\partial \tilde{U}_{xx}(\mathbf{p}_m, \mathbf{p}_n)}{\partial p_x} + (\beta_n^1 \beta_m^2 - \beta_n^2 \beta_m^1) \frac{\partial \tilde{U}_{xy}(\mathbf{p}_m, \mathbf{p}_n)}{\partial p_x} \right) \right], \quad (55)$$

$$\frac{\partial \tilde{U}_{xy}(\mathbf{p}_m, \mathbf{p}_m)}{\partial p_x} = \frac{1}{\alpha_m^2 \beta_m^1 - \alpha_m^1 \beta_m^2} \left[\alpha_m^2 - \sum_{n=1, n \neq m}^N \left((\alpha_n^1 \alpha_m^2 - \alpha_n^2 \alpha_m^1) \frac{\partial \tilde{U}_{xx}(\mathbf{p}_m, \mathbf{p}_n)}{\partial p_x} + (\beta_n^1 \alpha_m^2 - \beta_n^2 \alpha_m^1) \frac{\partial \tilde{U}_{xy}(\mathbf{p}_m, \mathbf{p}_n)}{\partial p_x} \right) \right], \quad (56)$$

The Eqs. (47, 52) are used to obtain:

$$\frac{\partial \tilde{U}_{xx}(\mathbf{p}_m, \mathbf{p}_m)}{\partial p_y} = \frac{1}{\alpha_m^1 \beta_m^2 - \alpha_m^2 \beta_m^1} \left[- \sum_{n=1, n \neq m}^N \left((\alpha_n^1 \beta_m^2 - \alpha_n^2 \beta_m^1) \frac{\partial \tilde{U}_{xx}(\mathbf{p}_m, \mathbf{p}_n)}{\partial p_y} + (\beta_n^1 \beta_m^2 - \beta_n^2 \beta_m^1) \frac{\partial \tilde{U}_{xy}(\mathbf{p}_m, \mathbf{p}_n)}{\partial p_y} \right) \right], \quad (57)$$

$$\frac{\partial \tilde{U}_{xy}(\mathbf{p}_m, \mathbf{p}_m)}{\partial p_y} = \frac{1}{\alpha_m^2 \beta_m^1 - \alpha_m^1 \beta_m^2} \left[- \sum_{n=1, n \neq m}^N \left((\alpha_n^1 \alpha_m^2 - \alpha_n^2 \alpha_m^1) \frac{\partial \tilde{U}_{xx}(\mathbf{p}_m, \mathbf{p}_n)}{\partial p_y} \right. \right. \\ \left. \left. + (\beta_n^1 \alpha_m^2 - \beta_n^2 \alpha_m^1) \frac{\partial \tilde{U}_{xy}(\mathbf{p}_m, \mathbf{p}_n)}{\partial p_y} \right) \right], \quad (58)$$

The Eqs. (48, 53) are used to obtain:

$$\frac{\partial \tilde{U}_{yx}(\mathbf{p}_m, \mathbf{p}_m)}{\partial p_x} = \frac{1}{\alpha_m^1 \beta_m^2 - \alpha_m^2 \beta_m^1} \left[- \sum_{n=1, n \neq m}^N \left((\alpha_n^1 \beta_m^2 - \alpha_n^2 \beta_m^1) \frac{\partial \tilde{U}_{yx}(\mathbf{p}_m, \mathbf{p}_n)}{\partial p_x} \right. \right. \\ \left. \left. + (\beta_n^1 \beta_m^2 - \beta_n^2 \beta_m^1) \frac{\partial \tilde{U}_{yy}(\mathbf{p}_m, \mathbf{p}_n)}{\partial p_x} \right) \right], \quad (59)$$

$$\frac{\partial \tilde{U}_{yy}(\mathbf{p}_m, \mathbf{p}_m)}{\partial p_x} = \frac{1}{\alpha_m^1 \beta_m^1 - \alpha_m^2 \beta_m^2} \left[- \sum_{n=1, n \neq m}^N \left((\alpha_n^1 \alpha_m^2 - \alpha_n^2 \alpha_m^1) \frac{\partial \tilde{U}_{yx}(\mathbf{p}_m, \mathbf{p}_n)}{\partial p_x} \right. \right. \\ \left. \left. + (\beta_n^1 \alpha_m^2 - \beta_n^2 \alpha_m^1) \frac{\partial \tilde{U}_{yy}(\mathbf{p}_m, \mathbf{p}_n)}{\partial p_x} \right) \right], \quad (60)$$

The equations (49, 54) are used to obtain:

$$\frac{\partial \tilde{U}_{yx}(\mathbf{p}_m, \mathbf{p}_m)}{\partial p_y} = \frac{1}{\alpha_m^1 \beta_m^2 - \alpha_m^2 \beta_m^1} \left[- \beta_m^1 - \sum_{n=1, n \neq m}^N \left((\alpha_n^1 \beta_m^2 - \alpha_n^2 \beta_m^1) \frac{\partial \tilde{U}_{yx}(\mathbf{p}_m, \mathbf{p}_n)}{\partial p_y} \right. \right. \\ \left. \left. + (\beta_n^1 \beta_m^2 - \beta_n^2 \beta_m^1) \frac{\partial \tilde{U}_{yy}(\mathbf{p}_m, \mathbf{p}_n)}{\partial p_y} \right) \right], \quad (61)$$

$$\frac{\partial \tilde{U}_{yy}(\mathbf{p}_m, \mathbf{p}_m)}{\partial p_y} = \frac{1}{\alpha_m^2 \beta_m^1 - \alpha_m^1 \beta_m^2} \left[- \alpha_m^1 - \sum_{n=1, n \neq m}^N \left((\alpha_n^1 \alpha_m^2 - \alpha_n^2 \alpha_m^1) \frac{\partial \tilde{U}_{yx}(\mathbf{p}_m, \mathbf{p}_n)}{\partial p_y} \right. \right. \\ \left. \left. + (\beta_n^1 \alpha_m^2 - \beta_n^2 \alpha_m^1) \frac{\partial \tilde{U}_{yy}(\mathbf{p}_m, \mathbf{p}_n)}{\partial p_y} \right) \right], \quad (62)$$

The selection of the constants c_x and c_y in reference solutions need some care. They should be selected in such a way that the denominators in the fractions on the right hand side of equations (55-62) are non-zero. By knowing all the elements A_{ij} and b_i of the system (40), we can determine the values of x_i . (i.e. α_n and β_n). Afterwards, we can calculate the solution of the governing equation from

$$u_\zeta(\mathbf{p}) = \sum_{n=1}^N \tilde{U}_{\zeta x}(\mathbf{p}, \mathbf{p}_n) \alpha_n + \sum_{n=1}^N \tilde{U}_{\zeta y}(\mathbf{p}, \mathbf{p}_n) \beta_n, \quad \zeta = x, y, \quad (63)$$

where \mathbf{p} is any point inside the domain or on the boundary.

3.3 Discretisation for a bi-material

We generalize the previous discussion for a bi-material problem. Consider that the domain Ω is split into two parts, Ω^I and Ω^{II} , bounded by boundaries Γ^I and Γ^{II} , and a common interface boundary $\Gamma^{I \cap II}$, as shown in Fig. 3. The material properties in both domains can be different in general. The governing equations are formally the same as Eqs. (1, 2) with

$$v = \begin{cases} v^I & \mathbf{p} \in \Omega^I, \\ v^{II} & \mathbf{p} \in \Omega^{II}, \end{cases} \quad u_\zeta = \begin{cases} u_\zeta^I & \mathbf{p} \in \Omega^I, \\ u_\zeta^{II} & \mathbf{p} \in \Omega^{II}, \end{cases} \quad \zeta = x, y, \quad (64)$$

where indexes I and II denote material properties in the domains Ω^I and Ω^{II} , respectively. The boundary conditions at the outer boundaries are given in the form, given by the Eqs. (3, 4). The boundary conditions at the interface between two materials $\Gamma^{I \cap II}$ are given in the form that represents the displacement continuity and traction equilibrium [Braccini and Dupeux (2012)]:

$$u_\zeta^I(\mathbf{p}) - u_\zeta^{II}(\mathbf{p}) = 0, \quad \zeta = x, y, \quad \mathbf{p} \in \Gamma^{I \cap II}, \quad (65)$$

$$t_\zeta^I(\mathbf{p}) + t_\zeta^{II}(\mathbf{p}) = 0, \quad \zeta = x, y, \quad \mathbf{p} \in \Gamma^{I \cap II}. \quad (66)$$

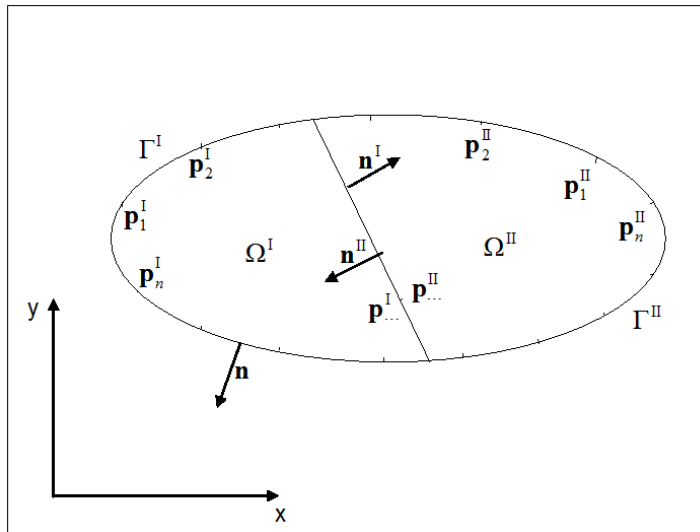


Figure 3: A bi-material with isotropic elastic, but in general different, material properties in domains Ω^I and Ω^{II}

The boundary $\Gamma^I \cup \Gamma^{I \cap II}$ is discretized in $N^I + N^{I \cap II}$ collocation points, and the boundary $\Gamma^{II} \cup \Gamma^{I \cap II}$ into $N^{II} + N^{I \cap II}$ collocation points, where $N = N^I + N^{II} + N^{I \cap II}$, and the number of collocation points on the interphase between two materials is $N^{I \cap II}$. The system (40) has in the bi-material problem a dimension of $2N + N^{I \cap II}$, respectively.

4 Numerical Examples

4.1 Example 1

In the first example (see Fig. 4), we consider a square with the side length $a = 2\text{m}$ centered around $p_x = 0\text{m}$, $p_y = 0\text{m}$. Elastic media is defined by $E = 1\text{N/m}^2$, $\nu = 0.3$.

We consider a solution of the Navier's equations in this square subject to the boundary conditions $\bar{u}_x = 0\text{m}$, $\bar{u}_y = 0\text{m}$ at point $p_x = 0\text{m}$, $p_y = -1\text{m}$, and $\bar{t}_x = 0\text{N/m}^2$, $\bar{t}_y = 0\text{N/m}^2$ on all other points of the south side of the square with $p_y = -1\text{m}$. On the north side of the square with $p_y = 1\text{m}$, uniform traction is prescribed $\bar{t}_x = 0\text{N/m}^2$, $\bar{t}_y = 1\text{N/m}^2$, and on the east $p_x = 1\text{m}$ and west $p_x = -1\text{m}$ sides $\bar{t}_x = 0\text{N/m}^2$, $\bar{t}_y = 0\text{N/m}^2$ is set. Such a unit uniform normal (in-plane) load acting along a single side of the square, was previously studied by Huang and Cruse (1994) when developing non-singular traction boundary integral equations in elasticity, and Panzeca, Fujita Yashima and Salerno (2001) by developing symmetric boundary element Galerkin method. The analytical solution is

$$u_x = -0.39p_x, \quad u_y = 0.91(p_y + 1) \tag{67}$$

$$\sigma_x = 0, \quad \sigma_y = 1, \quad \sigma_{xy} = 0. \tag{68}$$

A plot of the deformation, obtained with the analytical solution and the numerical solutions with MFS and NMFS is shown in Fig. 5 for the case with 100 nodes. The distance of the fictitious boundary from the true boundary for the MFS is set $R_M = 5d$, where d is the smallest distance between two nodes on the boundary. The radius of the circular disk for the distributed area source covering each node is set to $R = d/5$. The simple solution constants used in calculation of the diagonal coefficients are defined as $c_x = c_y = 4$ (see Fig. 16 in Appendix). When selecting $c_x = c_y = 0$ (see Fig. 17 in Appendix), we obtain for $\alpha_m^1 \beta_m^2 - \alpha_m^2 \beta_m^1$ a numerical value -7.8413×10^{-18} for point $p_x = 0\text{m}$, $p_y = 1\text{m}$ (both solutions have $\bar{u}_x(\mathbf{p}) = 0\text{m}$ in this point) and the solution obtained in this way is wrong (see Fig. 18, Appendix). So the two reference solutions should be selected in such a way that $\alpha_m^1 \beta_m^2 - \alpha_m^2 \beta_m^1 \neq 0$, $\alpha_m^2 \beta_m^1 - \alpha_m^1 \beta_m^2 \neq 0$; $m = 1, 2, \dots, N$.

The solution on boundary points are computed and compared with the analytical solutions. The root mean square (RMS) errors of the numerical solution are defined

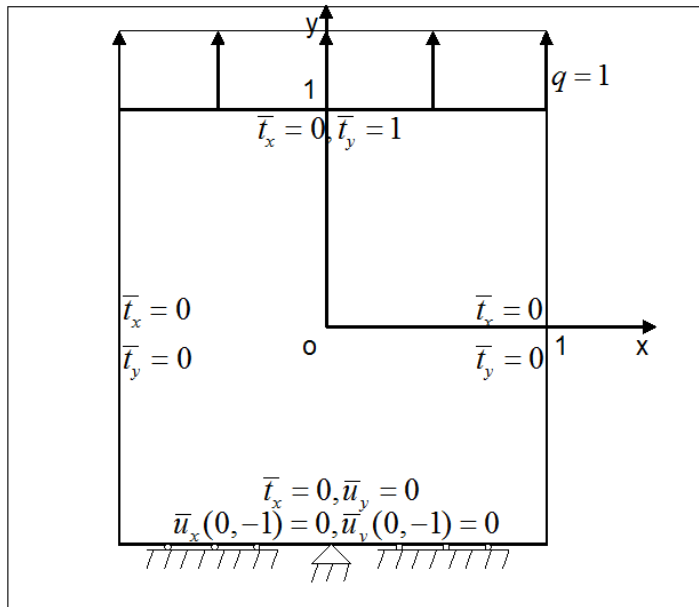


Figure 4: Example 1. Scheme of square subject to a uniform normal load.

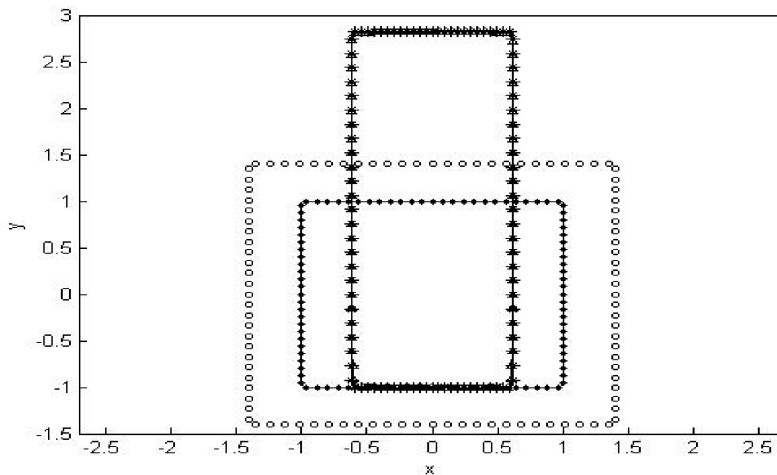


Figure 5: Example 1. The analytical solution and the numerical solution of MFS and NMFS with $N = 100$, $R = d/5$, $R_M = 5d$. (●: collocation points, ○: source points in MFS, +: analytical solution, ×: MFS solution, Δ:NMFS solution)

as

$$\zeta = \sqrt{\frac{1}{N} \sum_{n=1}^N (u_{\zeta n} - u_{\zeta n})^2}, \quad \zeta = x, y. \tag{69}$$

where $u_{\zeta k}$ and $u_{\zeta k}$, ($\zeta = x, y$) is the analytical and the numerical solution, respectively. The number of boundary nodes used is from 100 to 1924 (Odd-number of points should be used on the side in uniform discretization, since the middle point is fixed at $p_y = -1$ m).

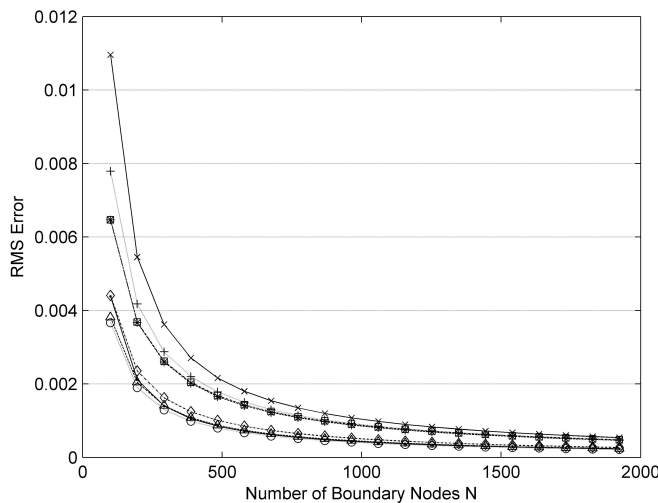


Figure 6: Example 1. The relationship between the RMS errors and the number of boundary nodes for different R , calculated by NMFS. (e_x : \bullet $R = d/3$, \circ $R = d/4$, Δ $R = d/5$, \diamond $R = d/6$; e_y : \times $R = d/3$, $+$ $R = d/4$, $*$ $R = d/5$, \square $R = d/6$)

Figure 6 shows RMS errors of the results obtained using the NMFS with different R . The errors are already less than 10^{-2} with $N = 196$ and the solution converges to the analytical solution with the increasing number of the nodes. The e_x and e_y are increasing with the decreasing R when $R < d/5$ (See Table 1). A comparison of the NMFS results with the MFS results is shown in Table 2 for $R = d/5$. Here it should be noted, that the MFS solution error is rather small, however the convergence is not uniform. This fact is due to the choice of the artificial boundary position, that was for all node arrangements $R_M = 5d$, and thus most probably not optimally varying.

Table 1: Example 1. RMS errors of NMFS solution as a function of different R .

num. of boundary nodes	$R = d/3$		$R = d/4$		$R = d/5$		$R = d/6$	
	e_x ($\times 10^{-2}$)	e_y ($\times 10^{-2}$)	e_x ($\times 10^{-2}$)	e_y ($\times 10^{-2}$)	e_x ($\times 10^{-2}$)	e_y ($\times 10^{-2}$)	e_x ($\times 10^{-2}$)	e_y ($\times 10^{-2}$)
100	0.4384	1.0959	0.3664	0.7791	0.3812	0.6467	0.4404	0.6466
196	0.2116	0.5453	0.1902	0.4175	0.2044	0.3672	0.2355	0.3681
292	0.1401	0.3620	0.1295	0.2873	0.1408	0.2595	0.1622	0.2616
388	0.1054	0.2707	0.0986	0.2197	0.1078	0.2017	0.1241	0.2042
484	0.0848	0.2162	0.0798	0.1782	0.0875	0.1654	0.1007	0.1681
580	0.0712	0.1799	0.0672	0.1500	0.0737	0.1405	0.0848	0.1431
676	0.0614	0.1541	0.0581	0.1297	0.0638	0.1222	0.0733	0.1247
772	0.0542	0.1347	0.0513	0.1142	0.0562	0.1082	0.0646	0.1107
868	0.0485	0.1197	0.0459	0.1021	0.0503	0.0972	0.0578	0.0995
964	0.0439	0.1077	0.0416	0.0924	0.0455	0.0882	0.0523	0.0905
1060	0.0402	0.0979	0.0380	0.0844	0.0416	0.0808	0.0477	0.0830
1156	0.0371	0.0897	0.0350	0.0776	0.0383	0.0746	0.0439	0.0767
1252	0.0344	0.0828	0.0325	0.0719	0.0355	0.0693	0.0407	0.0712
1348	0.0322	0.0769	0.0303	0.0670	0.0331	0.0647	0.0379	0.0666
1444	0.0302	0.0718	0.0284	0.0627	0.0310	0.0606	0.0355	0.0625
1540	0.0285	0.0673	0.0268	0.0589	0.0292	0.0571	0.0334	0.0589
1636	0.0269	0.0633	0.0253	0.0556	0.0275	0.0540	0.0315	0.0557
1732	0.0255	0.0598	0.0240	0.0526	0.0261	0.0512	0.0298	0.0528
1828	0.0243	0.0567	0.0228	0.0500	0.0248	0.0486	0.0283	0.0502
1924	0.0232	0.0538	0.0217	0.0476	0.0236	0.0464	0.0269	0.0479

4.2 Example 2

In the second numerical example, we use the same initial domain shape and the same material constants E and ν as in the Example 1. The boundary conditions on east, west, and south sides of the square are also the same as in the first example. On the north side of the square with $p_y = 1\text{m}$, bending traction is prescribed $\bar{t}_x = 0\text{N/m}^2$, $\bar{t}_y = (p_x/1\text{m})\text{N/m}^2$. Such a bending load, acting along a single side of the plate, was previously studied (like the Example 1) by Huang and Cruse (1994) and Panzeca, Fujita Yashima and Salerno (2001). The analytical solution is

$$u_x = -0.195p_x^2 - 0.445(p_y + 1)^2, \quad u_y = 0.91p_x(p_y + 1). \tag{70}$$

$$\sigma_x = 0, \quad \sigma_y = p_x, \quad \sigma_{xy} = 0 \tag{71}$$

A plot of the deformation, obtained with the analytical solution and the numerical solutions with MFS and NMFS is shown in Fig. 8 for the case with 100 nodes. R_M ,

Table 2: Example 1. RMS errors of MFS and NMFS solutions with $R_M = 5d$, $R = d/5$.

Number of boundary nodes (N)	MFS		NMFS	
	$e_x(\times 10^{-2})$	$e_y(\times 10^{-2})$	$e_x(\times 10^{-2})$	$e_y(\times 10^{-2})$
100	0.0001	0.0001	0.3812	0.6467
196	0.0000	0.0000	0.2044	0.3672
292	0.0000	0.0000	0.1408	0.2595
388	0.0067	0.0073	0.1078	0.2017
484	0.0086	0.0055	0.0875	0.1654
580	0.0001	0.0001	0.0737	0.1405
676	0.0000	0.0000	0.0638	0.1222
772	0.0005	0.0002	0.0562	0.1082
868	0.0007	0.0003	0.0503	0.0972
964	0.0181	0.0139	0.0455	0.0882
1060	0.0849	0.0556	0.0416	0.0808
1156	0.0002	0.0004	0.0383	0.0746
1252	0.0004	0.0005	0.0355	0.0693
1348	0.1234	0.0840	0.0331	0.0647
1444	0.0003	0.0003	0.0310	0.0606
1540	0.0003	0.0004	0.0292	0.0571
1636	0.0001	0.0002	0.0275	0.0540
1732	0.0000	0.0001	0.0261	0.0512
1828	0.0001	0.0001	0.0248	0.0486
1924	0.3393	0.2868	0.0236	0.0464

R , c_x , c_y , are set the same as in Example 1. The number of boundary nodes used is from 100 to 1924 and the results are shown in Table 4.

Figure 9 shows RMS errors of the results obtained by using the NMFS for different R . The solution converges to the analytical solution with the increasing number of the nodes, except in case with $R = d/3$. The e_x and e_y are increasing with the decreasing of R when $R < d/5$ (see Table 3). A comparison of the NMFS results with the MFS results is shown in Table 4 for $R = d/5$. Here it should be noted, that the MFS solution error is rather small, however the convergence is not uniform. This fact it is due to the choice of the artificial boundary position, that was for all node arrangement $R_M = 5d$, and thus most probably not optimally varying.

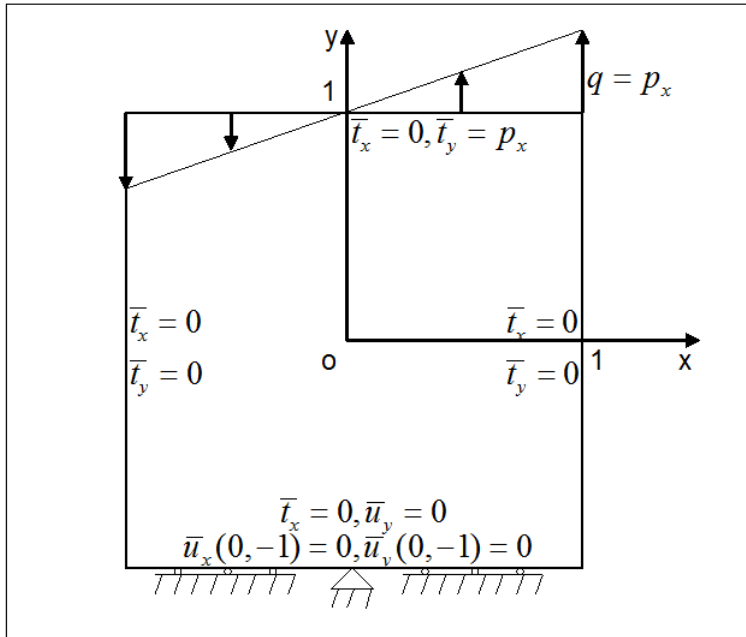


Figure 7: Example 2. A square plate subjected to a bending load.

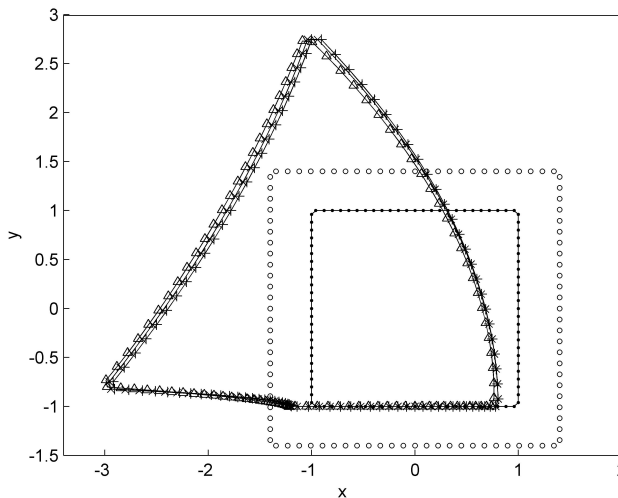


Figure 8: Example 2. The analytical solution and the numerical solution of MFS and NMFS with $N = 100$. $R = d/5$, $R_M = 5d$. (●: collocation points, ○: source points in MFS, +: analytical solution, ×: MFS solution, Δ: NMFS solution)

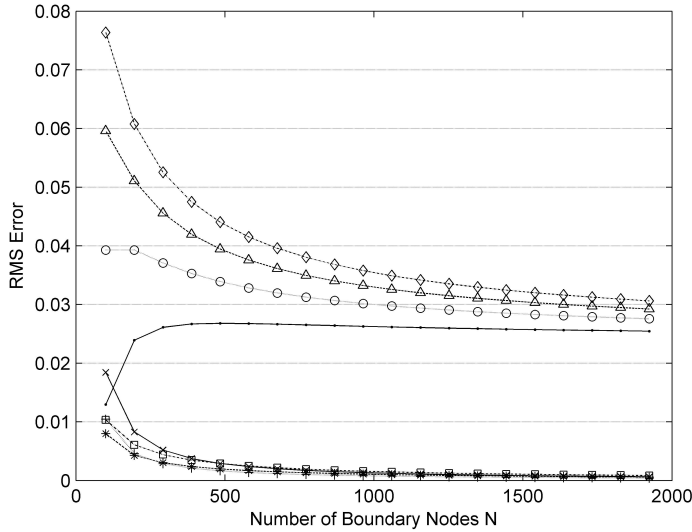


Figure 9: Example 2. The relationship between the RMS and the number of boundary nodes for different R , calculated by NMFS. (e_x : ● $R = d/3$, ○ $R = d/4$, $R = d/5$, ◇ $R = d/6$; e_y : × $R = d/3$, + $R = d/4$, * $R = d/5$, □ $R = d/6$)

4.3 Example 3

We consider a square with the side length $a = 2\text{m}$ in Example 3. We distinguish 3 sub-examples. In the first one, the whole square is occupied by one material, with the material properties $E = 1\text{N/m}^2$, $\nu = 0.3$. In the second one, the square is split into upper and lower parts with the same material properties as in the first example $E^I = E^{II} = 1\text{N/m}^2$, $\nu^I = \nu^{II} = 0.3$, and in the third one, the square is split as in the second one, but with more rigid material on the top, i.e. $E^I = 5\text{N/m}^2$, $E^{II} = 1\text{N/m}^2$, $\nu^I = 0.3$, $\nu^{II} = 0.3$. We consider the solution of the Navier's equations in this square subject to the boundary conditions $\bar{u}_x = 0\text{m}$, $\bar{u}_y = -0.1\text{m}$ on the north side with $p_y = 1\text{m}$, and $\bar{u}_x = 0\text{m}$, $\bar{u}_y = 0.1\text{m}$ on the south side with $p_y = -1\text{m}$, and $\bar{t}_x = 0\text{N/m}^2$, $\bar{t}_y = 0\text{N/m}^2$ on the east and west sides of the square with $p_x = -1\text{m}$ and $p_x = 1\text{m}$, respectively. A plot of the deformation, calculated with the defined three sub-examples is shown in Figures 10, 11, and 12, respectively. The following parameters have been used $R = d/5$, $R^I = d^I/5$, $R^{II} = d^{II}/5$, $c_x = c_y = c_x^I = c_y^I = c_x^{II} = c_y^{II} = 4$. The distance of the fictitious boundary from the true boundary in case of MFS is $R_M = 5d$, $R_M^I = 5d^I$, $R_M^{II} = 5d^{II}$.

Table 3: Example 2. RMS errors of NMFS solution as a function of different R .

num. of boundary nodes	$R = d/3$		$R = d/4$		$R = d/5$		$R = d/6$	
	e_x ($\times 10^{-2}$)	e_y ($\times 10^{-2}$)	e_x ($\times 10^{-2}$)	e_y ($\times 10^{-2}$)	e_x ($\times 10^{-2}$)	e_y ($\times 10^{-2}$)	e_x ($\times 10^{-2}$)	e_y ($\times 10^{-2}$)
100	1.2966	1.8427	3.9306	1.0462	5.9593	0.7990	7.6367	1.0348
196	2.3923	0.8280	3.9301	0.4572	5.1065	0.4276	6.0761	0.6090
292	2.6117	0.5201	3.7094	0.2878	4.5558	0.3037	5.2546	0.4415
388	2.6686	0.3751	3.5290	0.2097	4.1962	0.2388	4.7481	0.3491
484	2.6797	0.2917	3.3904	0.1651	3.9439	0.1980	4.4024	0.2898
580	2.6751	0.2379	3.2824	0.1364	3.7568	0.1697	4.1503	0.2484
676	2.6649	0.2004	3.1961	0.1163	3.6121	0.1489	3.9575	0.2178
772	2.6528	0.1729	3.1257	0.1015	3.4967	0.1328	3.8049	0.1940
868	2.6406	0.1518	3.0672	0.0901	3.4023	0.1200	3.6810	0.1751
964	2.6287	0.1353	3.0176	0.0810	3.3236	0.1095	3.5781	0.1597
1060	2.6175	0.1219	2.9752	0.0737	3.2568	0.1008	3.4912	0.1469
1156	2.6071	0.1109	2.9384	0.0676	3.1994	0.0934	3.4168	0.1360
1252	2.5974	0.1016	2.9061	0.0624	3.1495	0.0871	3.3522	0.1266
1348	2.5885	0.0938	2.8776	0.0581	3.1057	0.0816	3.2957	0.1185
1444	2.5802	0.0870	2.8522	0.0543	3.0669	0.0768	3.2458	0.1115
1540	2.5725	0.0812	2.8294	0.0509	3.0323	0.0725	3.2013	0.1052
1636	2.5654	0.0760	2.8088	0.0480	3.0011	0.0687	3.1614	0.0996
1732	2.5588	0.0715	2.7902	0.0454	2.9730	0.0653	3.1254	0.0946
1828	2.5526	0.0675	2.7731	0.0431	2.9475	0.0623	3.0928	0.0901
1924	2.5468	0.0639	2.7575	0.0410	2.9241	0.0595	3.0630	0.0860

4.4 Example 4

Example 4 is from the geometrical, material properties, discretization, as well as MFS and NMFS free parameters points of views equivalent to the Example 3. However, we consider the solution of the Navier’s equations subject to the boundary conditions $\bar{u}_x = -0.1\text{m}$, $\bar{u}_y = 0\text{m}$ on the north side with $p_y = 1\text{m}$, and $\bar{u}_x = 0.1\text{m}$, $\bar{u}_y = 0\text{m}$ on the south side with $p_y = -1\text{m}$; and $\bar{t}_x = 0\text{N/m}^2$, $\bar{t}_y = 0\text{N/m}^2$ on the east and west sides of the square with $p_x = -1\text{m}$ and $p_x = 1\text{m}$, respectively. A plot of the deformation, calculated with the three sub-examples is shown in Figures 13, 14, and 15, respectively.

Table 4: Example 2. RMS errors of MFS and NMFS solutions with $R_M = 5d$, $R = d/5$.

Number of boundary nodes (N)	MFS		NMFS	
	$e_x(\times 10^{-2})$	$e_y(\times 10^{-2})$	$e_x(\times 10^{-2})$	$e_y(\times 10^{-2})$
100	2.3656	0.0002	5.9593	0.7990
196	4.5717	5.3138	5.1065	0.4276
292	3.5939	1.4795	4.5558	0.3037
388	2.3657	0.0037	4.1962	0.2388
484	2.3710	0.0038	3.9439	0.1980
580	2.0706	1.1063	3.7568	0.1697
676	1.3096	1.1845	3.6121	0.1489
772	1.8889	2.4678	3.4967	0.1328
868	0.8536	0.4878	3.4023	0.1200
964	2.4082	0.0282	3.3236	0.1095
1060	2.3126	0.0347	3.2568	0.1008
1156	2.3640	0.0016	3.1994	0.0934
1252	2.3620	0.0196	3.1495	0.0871
1348	2.3589	0.0055	3.1057	0.0816
1444	2.3638	0.0016	3.0669	0.0768
1540	2.3654	0.0008	3.0323	0.0725
1636	2.4276	0.3268	3.0011	0.0687
1732	1.8726	2.3862	2.9730	0.0653
1828	1.6583	1.7767	2.9475	0.0623
1924	2.3374	0.0267	2.9241	0.0595

Table 5: Example 3. The results of MFS and NMFS for example from Fig. 12.

p_x	p_y	MFS		NMFS	
		$u_x(\times 10^{-2})$	$u_y(\times 10^{-2})$	$u_x(\times 10^{-2})$	$u_y(\times 10^{-2})$
0	0.9000	0.0000	-9.7508	0.0006	-9.5376
0	0.7000	0.0000	-9.2060	0.0027	-9.0131
0	0.5000	0.0000	-8.5927	0.0056	-8.4228
0	0.3000	0.0000	-7.9061	0.0089	-7.7673
0	0.1000	0.0000	-7.1430	0.0125	-7.0381
0	-0.1000	0.0000	-5.0788	0.0142	-4.8667
0	-0.3000	0.0000	-1.6275	0.0119	-1.5403
0	-0.5000	0.0000	1.8972	0.0085	1.8589
0	-0.7000	0.0000	5.3340	0.0050	5.1709
0	-0.9000	0.0000	8.5295	0.0018	8.2406

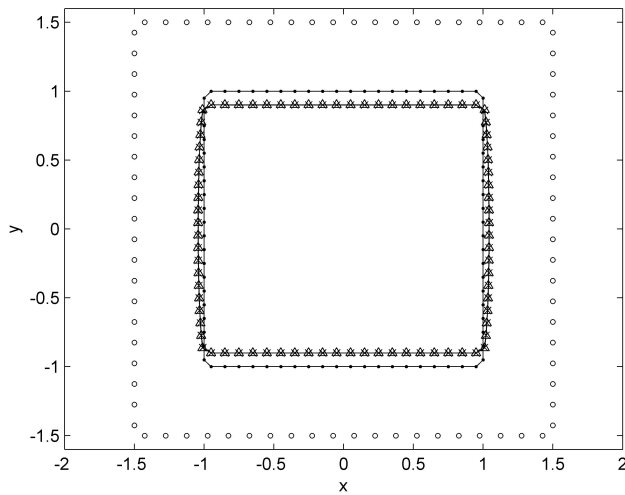


Figure 10: Example 3. The deformation, calculated with MFS and NMFS, for a one-domain case with $E = 1N/m^2$, $\nu = 0.3$ and $N = 80$. (●: collocation points, ○: source points, ×: MFS solution, △: NMFS solution)

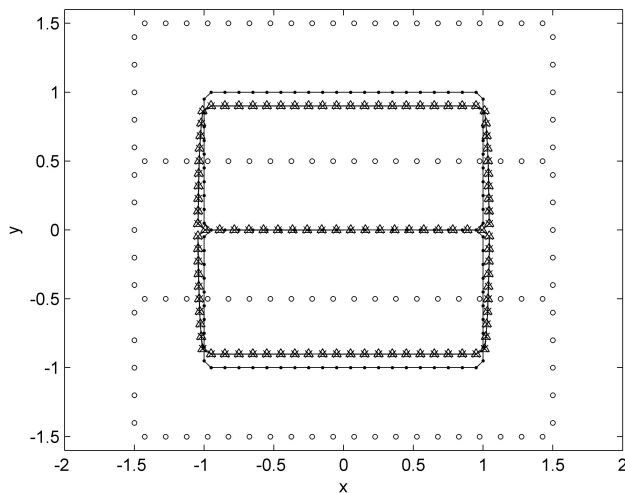


Figure 11: Example 3. The deformation, calculated with MFS and NMFS, for a bi-material case with material properties $E^I = 1N/m^2$, $E^{II} = 1N/m^2$, $\nu^I = 0.3$, $\nu^{II} = 0.3$, and $N = 100$, $N^{I \cap II} = 20$. (●: collocation points, ○: source points, ×: MFS solution, △: NMFS solution)

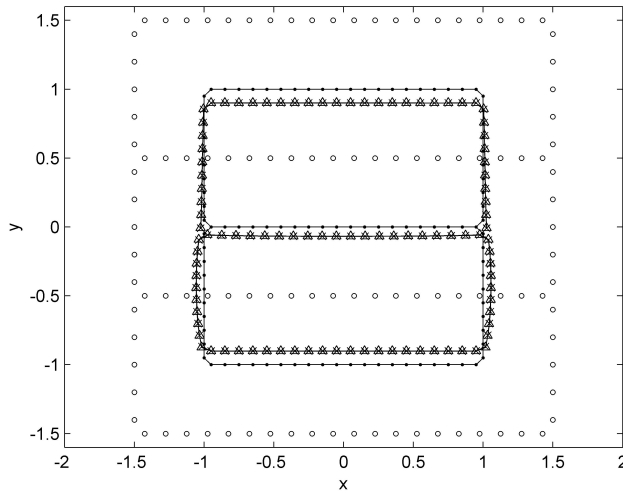


Figure 12: Example 3. The deformation, calculated with MFS and NMFS, for a bi-material case with material properties $E^I = 5N/m^2$, $E^{II} = 1N/m^2$, $\nu^I = 0.3$, $\nu^{II} = 0.3$, and $N = 100$, $N^{I \cap II} = 20$. (●: collocation points, ○: source points, ×: MFS solution, Δ :NMFS solution)

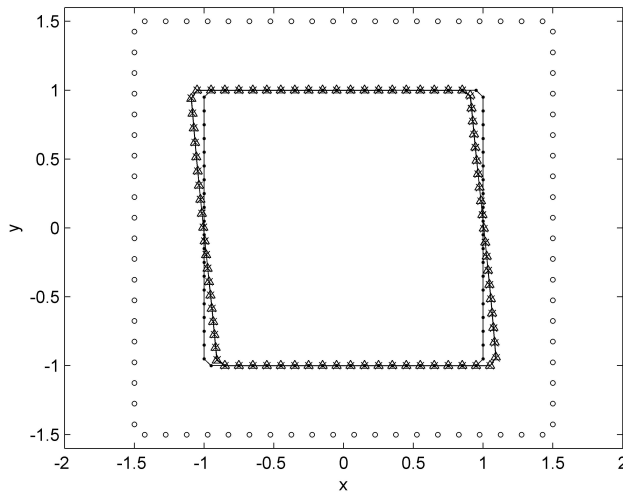


Figure 13: Example 4. The deformation , calculated with MFS and NMFS, for a one-domain case with material properties $E = 1N/m^2$, $\nu = 0.3$, and $N = 80$. (●: collocation points, ○: source points, ×: MFS solution, Δ :NMFS solution)

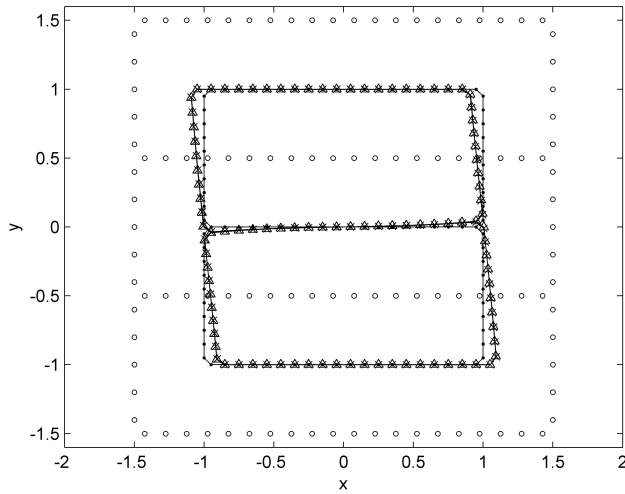


Figure 14: Example 4. The deformation, calculated with MFS and NMFS, for a bi-material case with material properties $E^I = 1N/m^2$, $E^{II} = 1N/m^2$, $\nu^I = 0.3$, $\nu^{II} = 0.3$, and $N = 100$, $N^{I \cap II} = 20$. (\bullet : collocation points, \circ : source points, \times : MFS solution, Δ : NMFS solution)

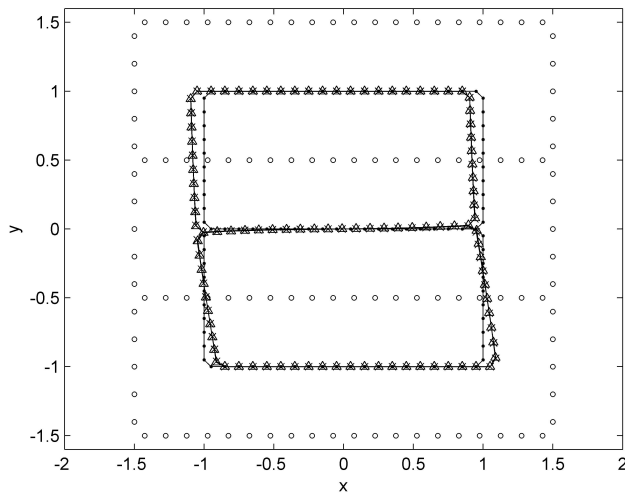


Figure 15: Example 4. The deformation, calculated with MFS and NMFS, for a bi-material case with material properties $E^I = 5N/m^2$, $E^{II} = 1N/m^2$, $\nu^I = 0.3$, $\nu^{II} = 0.3$, and $N = 100$, $N^{I \cap II} = 20$. (\bullet : collocation points, \circ : source points, \times : MFS solution, Δ : NMFS solution)

Table 6: Example 4. The results of MFS and NMFS for example from Fig. 15.

P_x	P_y	MFS		NMFS	
		$u_x(\times 10^{-2})$	$u_y(\times 10^{-2})$	$u_x(\times 10^{-2})$	$u_y(\times 10^{-2})$
0	0.9000	-9.7338	0.0000	-9.7120	-0.0018
0	0.7000	-9.0963	0.0000	-9.0231	-0.0054
0	0.5000	-8.3310	0.0000	-8.2141	-0.0099
0	0.3000	-7.4769	0.0000	-7.3302	-0.0161
0	0.1000	-6.5940	0.0000	-6.4374	-0.0243
0	-0.1000	-4.4547	0.0000	-4.2997	-0.0277
0	-0.3000	-1.0468	0.0000	-0.8980	-0.0231
0	-0.5000	2.3213	0.0000	2.4442	-0.0170
0	-0.7000	5.5617	0.0000	5.6458	-0.0103
0	-0.9000	8.5810	0.0000	8.6164	-0.0036

5 Discussion

The numerical Examples 1 and 2 show good agreement of both NMFS and MFS solutions with the analytical solution. The numerical Examples 3 and 4 show good agreement between the solution for a one domain region and a solution recalculated with the two regions in ideal mechanical contact and with the same material properties (compare Fig.10 with Fig. 11, and Fig. 13 with 14). The maximum absolute difference in displacements between values in Fig. 10 and Fig. 11 at the outer boundary are $u_x = 0.0011\text{m}$, $u_y = 9.2544 \times 10^{-4}\text{m}$, and between Fig.13 and Fig. 14 $u_x = 4.3003 \times 10^{-4}\text{m}$, $u_y = 0.0014\text{m}$, respectively. The Examples 3 and 4 demonstrate the expected behavior of the solution when a bi-material with different elasticity parameters is deformed (see Fig. 12 and Fig. 15).

6 Conclusions

A new NMFS (termed also BDSM by Liu (2010)), is extended in the present paper to solve the two-dimensional linear elasticity problems. In this approach, the singular values of fundamental solution are integrated over small circles, so that the coefficients of the system of equations can be evaluated analytically in case of displacement boundary conditions, leading to extremely simple computer implementation of this method. In case of traction boundary conditions, two more systems of equations with the same size as the original MFS problem have to be solved to determine the respective desingularized derivatives. The NMFS essentially gives the same results as the classical MFS. It has the advantage that the

artificial boundary is not present, however on the expense of solving three times the systems of algebraic equations in comparison with only one solution in MFS. The results obtained using MFS and NMFS are compared to each other. Sensitivity analyses of the influence of density of points are done and representative numerical examples for single and bi-materials have been performed. The NMFS method presented in this paper is very general and it can be adapted or extended to handle many related problems, such as three dimensional elasticity, anisotropic elasticity, and multi-body problems which all represent directions of our further investigation. The advantage of not having to generate the artificial boundary is particularly welcome in these type of problems. The developed method most probably represents a simplest known way how to numerically cope with these type of problems. The method will be used in the future for calculation of multigrain deformation [Mura (1987)] problems in metals, with realistic grain shapes, obtained from the microscope images. It represents an alternative to the recent development direction of T-Trefftz Voronoi cell finite elements [Dong and Atluri (2011a); Dong and Atluri (2011b); Dong and Atluri (2013)] for macro- & micromechanics of inhomogeneous media with inclusions and cracks. The problems with arbitrarily shaped inhomogeneities in the form of elastic inclusions, rigid inclusions and voids, as discussed in [Dong and Atluri, (2012)] will be numerically implemented next.

Acknowledgement

This work was funded by the Slovenian Research Agency (ARRS) in the framework of basic research project J2-4093 Development and application of advanced numerical methods in study of karst processes, and research programme P2-0379 Modelling and simulation of materials and processes. The Centre of Excellence for Biosensors, Instrumentation and Process Control (COBIK) is an operation financed by the European Union, European Regional Development Fund and Republic of Slovenia, Ministry of Education, Science Culture and Sport. The authors would like to thank Professors Jan and Vladimir Sladek for useful suggestions regarding the paper.

References

- Aleksidze M. A.** (1991): *Fundamentalnye funktsii v priblizhennykh resheniyakh granichnykh zadach [Fundamental functions in approximate solutions of boundary value problems]*. Spravochnaya Matematicheskaya Biblioteka [Mathematical Reference Library], "Nauka", Moscow. (in Russian); (with an English summary).
- Berger J. R.; Karageorghis A.** (2001): The method of fundamental solutions for layered elastic materials. *Engineering Analysis with Boundary Elements*, vol. 25,

pp. 877-886.

Berger J. R.; Karageorghis A.; Martin P. A. (2007): Stress intensity factor computation using the method of fundamental solutions: mixed-mode problems. *International Journal for Numerical Methods in Engineering*, vol. 69, pp.469-483

Beskos D. E. (1987): *Boundary Element Methods in Mechanics*. Elsevier Science Publishers B. V. North-Holland.

Braccini M.; Dupeux M. (2012): *Mechanics of Solid Interfaces*. Wiley, New York.

Burgess G.; Maharejin E. (1984): A comparison of the boundary element and superposition methods. *Computers & Structures*, vol. 19, pp. 697-705.

Chen K. H.; Kao J. H.; Chen J. T.; Young D. L.; Lu M. C. (2006): Regularized meshless method for multiply-connected-domain Laplace problems. *Engineering Analysis with Boundary Elements*, vol. 30, pp. 882-896.

Chen C. S.; Karageorghis A.; Smyrlis Y. S. (2008): The Method of Fundamental Solutions - A Meshless Method, *Dynamic Publishers*, Atlanta.

Chen W.; Wang F. Z. (2010): A method of fundamental solutions without fictitious boundary. *Engineering Analysis with Boundary Elements*, vol. 34, pp. 530-532.

Chen W.; Lin J.; Wang F. Z. (2011): Regularized meshless method for nonhomogeneous problems. *Engineering Analysis with Boundary Elements*, vol. 35, pp. 253-257.

Dong L.; Atluri S. N. (2011a): A simple procedure to develop efficient & stable Hybrid/Mixed elements, and Voronoi cell finite elements for macro- & micromechanics. *CMC: Computers, Materials & Continua*, vol. 24, pp. 61-104.

Dong L.; Atluri S. N. (2011b): Development of T-Trefftz four- node quadrilateral and Voronoi cell finite elements for macro- & micromechanical modeling of solids. *CMES: Computers Modeling in Engineering & Sciences*, vol. 81, pp. 69-118.

Dong L.; Atluri S. N. (2012): T-Trefftz Voronoi cell finite elements with elastic/rigid inclusions or voids for micromechanical analysis of composite and porous materials. *CMES: Computers Modeling in Engineering & Sciences*, vol. 83, pp. 183-219.

Dong L.; Atluri S. N. (2013): SGBEM Voronoi cells (SVCs) with embedded arbitrary shaped inclusions, voids, and/or cracks for micromechanical modeling of heterogenous materials. *CMC: Computers Materials Continua*, vol. 33, pp. 111-154.

Fairweather G.; Karageorghis A. (1998): The method of fundamental solutions for elliptic boundary value problems. *Advances in Computational Mathematics*, vol. 9, pp. 69-95.

Fenner R. T. (2001): A force field superposition approach to plane elastic stress and strain analysis, *Journal of Strain Analysis for Engineering Design*, vol. 36, pp. 517-529.

Golberg M. A.; Chen C. S. (1997): *Discrete Projection Methods for Integral Equations*, Computational Mechanics Publications, Southampton.

Golberg M. A., Chen C. S. (1999): The method of fundamental solutions for potential, Helmholtz and diffusion problems, in: *Boundary Integral Methods: Numerical and Mathematical Aspects, Computational Engineering*, vol. 1. WIT Press/Computational Mechanics Publications, Boston, MA, pp. 103-176.

Gu Y.; Chen W.; Zhang C. Z. (2011): Singular boundary method for solving plane strain elastostatic problems. *International Journal of Solids and Structures*, vol. 48, pp. 2549-2556.

Huang G.; Cruse T. A. (1994): On the non-singular traction-BIE in elasticity. *International Journal of Numerical Methods in Engineering*. vol. 37, pp. 2041-2072.

Karageorghis A.; Fairweather G. (2000): The method of fundamental solutions for axisymmetric elasticity problems. *Computational Mechanics*, vol. 25, pp. 524-532.

Karageorghis A.; Poullikkas A.; Berger J. R. (2006): Stress intensity factor computation using the method of fundamental solutions. *Computational Mechanics*, vol. 37, pp. 445-454.

Kolodziej J. A. (1987): Review of applications of boundary collocation methods in mechanics of continuous media. *Solid Mechanics Archives*, vol. 12, pp. 187-231.

Kolodziej J. A. (2001): *Zastosowanie metody kollokacji brzegowej w zagadnieniach mechaniki [Applications of the Boundary Collocation Method in Applied Mechanics]*, Wydawnictwo Politechniki Poznańskiej, Poznań, (in Polish).

Kupradze V. D. (1964): On a method of solving approximately the limiting problems of mathematical physics. *Ž. Vyčisl. Mat. i Mat. Fiz.* vol. 4, pp. 1118-1121.

Kupradze V. D.; Aleksidze M. A. (1964): The method of functional equations for the approximate solution of certain boundary value problems. *Comput. Methods Math. Phys.* vol. 4, pp. 82-126.

Kupradze V. D.; Gegelia T. G.; Bashaeshvili M. O.; Burchuladze T. V. (1976): *Trekhmernye zadachi matematicheskoi teorii uprugosti i termouprugosti [Three-dimensional problems in the mathematical theory of elasticity and thermoelasticity.]*, Izdat. "Nauka", Moscow, (in Russian).

Liu Y. J. (2010): A new boundary meshfree method with distributed sources. *Engineering Analysis with Boundary Elements*, vol. 34, pp. 914-919.

- Maharejin E.** (1985): An extension of the superposition method for plane anisotropic elastic bodies. *Computers & Structures*, vol. 21, pp. 953-958.
- Marin L.** (2011): Relaxation procedures for an iterative MFS algorithm for two-dimensional steady-state isotropic heat conduction Cauchy problems. *Engineering Analysis with Boundary Elements*, vol. 35, pp. 415-429.
- Marin L.; Lesnic D.** (2004): The method of fundamental solutions for the Cauchy problem in two-dimensional linear elasticity. *International Journal of Solids and Structures*, vol. 41, pp. 3425-3438.
- Mura T.** (1987): *Micromechanics of Defects in Solids*. 2ed, Martinus Nijhoff Publishers, Netherlands.
- Panzeca T.; Fujita Yashima H.; Salerno M.** (2001): Direct stiffness matrices of BEs in the Galerkin BEM formulation. *European Journal of Mechanics - A/Solids*, vol. 20, pp. 277-298
- Patterson C.; Sheikh M. A.** (1982): On the use of fundamental solutions in Trefftz method for potential and elasticity problems, in: C.A. Brebbia (Ed.), *Boundary Element Methods in Engineering*, Proceedings of the Fourth International Seminar on Boundary Element Methods, Springer, New York, pp. 43-54.
- Perne M.; Šarler B.; Gabrovšek F.** (2012): Calculating transport of water from a conduit to the porous matrix by boundary distributed source method, *Engineering Analysis with Boundary Elements*, vol.36, pp. 1649-1659.
- Poullikkas A.; Karageorghis A.; Georgiou G.** (2002): The method of fundamental solutions for three-dimensional elastostatics problems, *Computers & Structures*, vol. 80, pp. 365-370.
- Raamachandran J.; Rajamohan C.** (1996): Analysis of composite plates using charge simulation method, *Engineering Analysis with Boundary Elements*, vol. 18, pp. 131-135.
- Redekop D.** (1982): Fundamental solutions for the collocation method in planar elastostatics, *Applied Mathematical Modelling*, vol. 6, pp. 390-393.
- Redekop D.; Thompson J. C.** (1983): Use of fundamental solutions in the collocation method in axisymmetric elastostatics, *Computers & Structures*, vol. 17, pp. 485-490.
- Redekop D.; Cheung R. S. W.** (1987): Fundamental solutions for the collocation method in three-dimensional elastostatics, *Computers & Structures*, vol. 26, pp. 703-707.
- Šarler B.** (2009): Solution of potential flow problems by the modified method of fundamental solutions: formulations with the single layer and the double layer fundamental solutions. *Engineering Analysis with Boundary Elements*, vol. 33, pp.

1374-1382.

Smyrlis Y.S. (2009): Applicability and applications of the method of fundamental solutions, *Mathematics of Computation*, vol. 78, pp. 1399-1434.

Tsai C. C. (2007): The method of fundamental solutions for three-dimensional elastostatic problems of transversely isotropic solids. *Engineering Analysis with Boundary Elements*. vol. 31, pp. 586-594.

Young D. L.; Chen K. H.; Chen J. T.; Kao J. H. (2007): A modified method of fundamental solutions with source on the boundary for solving Laplace equations with circular and arbitrary domains. *CMES: Computer Modeling in Engineering & Sciences*, vol. 19, pp. 197-222.

Young D. L.; Chen K. H.; Lee C. W. (2005): Novel meshless method for solving the potential problems with arbitrary domain. *Journal of Computational Physics*, vol. 209, pp. 290-321.

Appendix

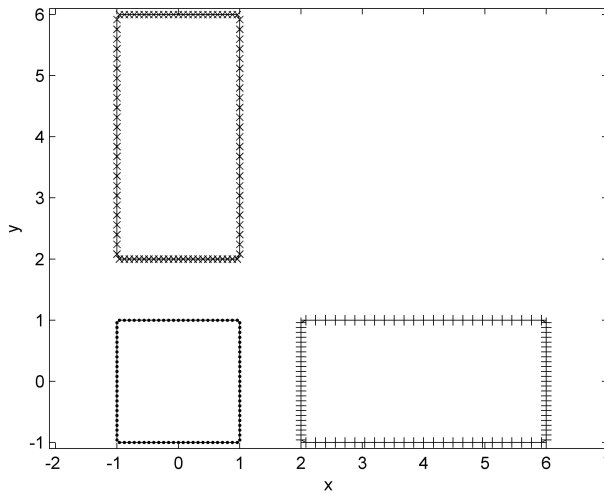


Figure 16: Example 1. The known two reference solutions of the governing equation (\bullet : initial layout, $+$: $\bar{u}_x(\mathbf{p}) = p_x + 4, \bar{u}_y(\mathbf{p}) = 0, \times: \bar{u}_x(\mathbf{p}) = 0, \bar{u}_y(\mathbf{p}) = p_y + 4.$), used in calculation of the desingularized values of fundamental solution in traction boundary condition poits, that give proper NMFS solution.

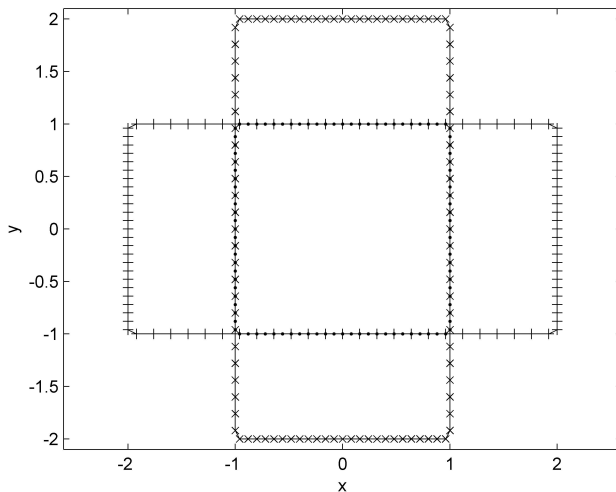


Figure 17: Example 1. The known two reference solutions of the governing equation (•: initial layout, +: $\bar{u}_x(\mathbf{p}) = p_x, \bar{u}_y(\mathbf{p}) = 0, \times: \bar{u}_x(\mathbf{p}) = 0, \bar{u}_y(\mathbf{p}) = p_y$), used in calculation of the desingularized values of fundamental solution in traction boundary condition points, that give erroneous NMFS solution.

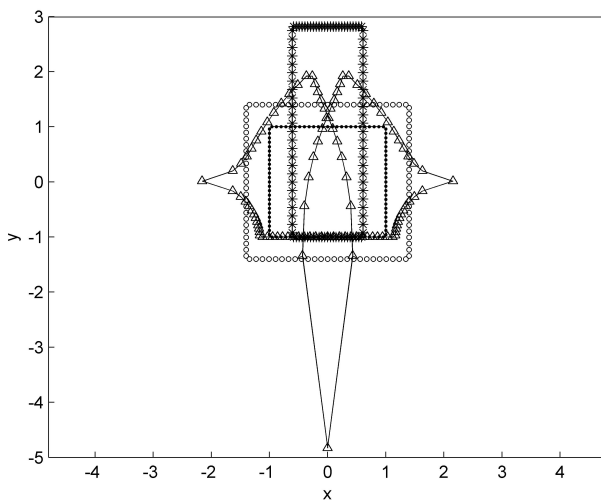


Figure 18: Example 1. The analytical solution, the numerical solution with MFS and the erroneous numerical solution with NMFS with $N = 100$ and $c_x = c_y = 0$. (•: collocation points, ○: source points in MFS, +: analytical solution, ×: MFS solution, Δ :NMFS solution)